

Study of a Downwash Caused by a Hovering Rotor in Ground Effect

Yasutada Tanabe, Shigeru Saito

Japan Aerospace Exploration Agency (JAXA),
7-44-1 Jindaiji Higashi-machi, Chofu, Tokyo 182-8522, JAPAN
e-mail: tan@chofu.jaxa.jp

and

Naoko Ooyama, Katsumi Hiraoka

Graduate School, Tokai University
Kita-Kaname 1117, Hiratsuka, Kanagawa 259-1207, JAPAN

Abstract

Helicopter is allowed to land onto a highway during emergency medical service (EMS) recently in Japan. While there are concerns about the influence of the caused downwash on the surface vehicles, especially the motorcycles, relatively strict regulation is set for the landing areas. An investigation group was organized by ATEC (Association of Air Transport Engineering and Research) in Japan to study the detailed structure of the downwash caused by a hovering helicopter and its influence on the surface vehicles. Simulation using CFD methods were carried out and combined with the jet-blowing experimental results, a general downwash model for a hovering rotor in ground effect is proposed in this study.

Nomenclature

Abbreviations

CFD	Computational Fluid Dynamics
HART	Higher harmonic control Aeroacoustic Rotor Test
WJM	Wall Jet Model induced by rotor in hover
MUSCL	Monotone Upstream-Centered Scheme for Conservation Laws
TVD	Total Variation Diminishing
SHUS	Simple High-resolution Upwing Scheme
FCMT	Fourth-order Compact MUSCL TVD
AUSM	Advection Upstream Splitting Method
FDS	Flux Difference Splitting
CFL	Courant-Friedrich-Lewy
IGE	In Ground Effect
OGE	Out of Ground Effect
EMS	Emergency Medical Service
MPI	Message Passing Interface

Symbols

A	rotor area, $= \pi R^2$
C_T	rotor thrust coefficient

C_Q	rotor torque coefficient
D	rotor diameter, $=2R$
\tilde{F}	numerical flux
N	metrics vector for cell surface pressure
Q	rotor shaft torque, Nm
Q	conservative variable vector of flow
R	rotor radius
T	rotor thrust, N
U, V	wind at ground vehicle axis
V_{i0}	uniform induced velocity at rotor plane in hover based on momentum theory
X, Y, Z	fixed axes, origin at rotor center
b	coefficient in MUSCL limiter; also used as length scale for wall jet
b_l	coefficient in MUSCL slope limiter
c	blade chord
h	total enthalpy of flow
h_R	rotor height from ground
p	pressure
r	radial distance from rotor center
u, v, w	velocity components of flow in X, Y, Z direction respectively
Φ	primitive variable vector in Euler equations
Δ	difference operator
θ_0	collective pitch angle, deg
ρ	flow density

Superscripts

L	value at left side of cell boundary
R	value at right side of cell boundary

Subscripts

i	grid coordinate index, spanwise on blade
j	grid coordinate index, chordwise on blade
k	thickwise coordinate index of blade grid
n	normal to cell surface

Introduction

It is well known that while a helicopter is flying at very low air speed near the ground, the wake from the helicopter rapidly change its structure from a ideal hovering state to a large roll-up flow around the helicopter which causes the brown-out when onto a sandy surface and white-out while onto a snowy surface. This also causes large variations in the downwash velocities along the ground surface in the vicinity. Considering the influence of the downwash on the ground traffics, strongest wall jet is observed when the helicopter is in a hovering flight near the ground.

Helicopters are widely used for emergency medical services (EMS). It is very effective to send a doctor with a nurse directly onto a traffic accident site to save the casualties and has been proved to reduce the death-rate significantly. However, there are still concerns about the influences on the nearby cars and motorcycles of the downwash induced by the helicopter during landing and take-off on the highway. Detailed understanding of the downwash structure thus will be helpful for the safe operation of helicopter onto the highway while the traffic on the neighboring opposite car lane is not stopped.

Downwash on the ground induced by a hovering rotor is a somewhat classical problem for helicopter industry but the available published literatures of measurement is quite limited. The measurement done by NASA (Ref. 1) with a H-13 helicopter back in 1961 still remains the often referenced source of such experiments. Because the natural wind may significantly influence the downwash structure, it is very difficult if not impossible to perform a reliable measurement with small deviations. The flowfield itself have instinct unsteady features

that make it more difficult to distinguish that from the fluctuations caused by the environmental winds.

There are more experiments with small model rotors reported on the ground effect and its influence on the wall jet on the ground. Iboshi et al. (Ref. 2) have done a series of such measurements with a pitot tube and show the velocity profiles near the rotor are significant influenced by the rotor height but suggested a strong similarity with different thrust while scaled with the uniform induced velocities calculated with simple momentum theory.

Currently, Leishman et al. (Ref. 3) performed a detailed flow structure measurements with a dual-laser technique of a hovering rotor in ground effect and clarified the unsteady structure of the flow caused by the vortices shed from the tip of the rotor blade especially in the vicinity of the rotor. It is also indicated that the vortices dissipate fast inside the wall jet away from the rotor and the fluctuations of the flow speed decays accordingly.

In Japan, EMS helicopter (called Doctor-Heli in Japan) is allowed to directly land onto the highway just very recently. The concern about the influence of the downwash on the ground traffic at the opposite lanes arises. A comparatively strict regulation of the ground traffic on the neighbor opposite lane is testingly carried on. With clearer understanding of the structure of the helicopter downwash and its effect on the ground vehicles, a more reasonable regulation is hopefully to be established which should improve the operativity of the EMS helicopters in Japan. An investigation group was organized by ATEC (Association of Air Transport Engineering and Research) in Japan to study the detailed structure of the downwash caused by a hovering helicopter and its influence on the surface vehicles, especially the motorcycles. Simulations using CFD methods were carried out in JAXA (Japan Aerospace eXploration Agency) for a hovering rotor above a flat plane at various heights from the ground. Away from the rotor, considering the similarity of the flowfield with the jet-blowing, it is proposed to switch to the jet-blowing experimental results, while the swirl velocity component from the CFD results is remained. Finally, a general downwash model for a hovering rotor in ground effect is proposed, which offers a first order of

estimation of the velocity distribution and direction of the airflow parallel with the ground at any position from the center of the hovering rotor. It is suggested to use this simple downwash model for further analysis of the influence of the downwash from a hovering rotor on the ground traffic.

CFD Simulation

A CFD code referred as JAXA_ov3d (Ref. 4) based on the moving overlapped grids method is used and its main features are as follows:

A fine inner background Cartesian grid is used to resolve the vortex wake of the rotor in addition to the wider outer background Cartesian grid. SOH type blade grid is used mainly for shape fidelity.

- Divided time steps between grids allow correct time advancing based on blade azimuth angle under respective CFL number limits set for each grid where different numerical scheme could be used.
- Fully unsteady Euler/NS formulations so the blade motion effects are reflected through grid moving and deforming only.
- A Simple High-resolution Upwind Scheme (SHUS) (Ref. 5) is used for the Cartesian background grids with 4th order accuracy in space and also an explicit 4 stages Runge-Kutta integration scheme (Ref. 6) in time is used.
- A robust 2nd-order implicit TVD scheme (Ref. 7) is used for the moving blade grids allowing larger CFL number.
- Standard MPI routines are adapted for parallel computing processes.

SHUS (Simple High-resolution Upwind Scheme) scheme is developed by Shima et al. (Ref. 5) as an improvement from AUSM (Advection Upstream Splitting Method) scheme (Ref. 8) by using Roe's FDS mass flux instead of that in original AUSM scheme. The overshoot at shock front is eliminated and this scheme is more robust. Combined with a 4th-order compact MUSCL extrapolation method, this scheme is very stable and has good preservation of vortex (Ref. 9).

The Euler equations can be written in a integral form as follows:

$$\int_V \mathbf{Q} dv + \int_{\partial V} \tilde{\mathbf{F}} ds = 0 \quad (1)$$

V is the volume and ∂V is the surface of the control volume cell in consideration. Here,

$$\mathbf{Q} = \begin{pmatrix} \rho \\ \rho u \\ \rho v \\ \rho w \\ e \end{pmatrix} \quad (2)$$

$$\tilde{\mathbf{F}} = m\Phi + p\mathbf{N} \quad (3)$$

$$\Phi = \begin{pmatrix} 1 \\ u \\ v \\ w \\ h \end{pmatrix}, \quad \mathbf{N} = \begin{pmatrix} 0 \\ x_n \\ y_n \\ z_n \\ 0 \end{pmatrix} \quad (4)$$

$$m = \rho V_n, \quad V_n = x_n u + y_n v + z_n w \quad (5)$$

where $\rho, u, v, e, p, h = (e + p) / \rho$ represent density, velocity in x, y and z direction, total energy per unit volume, pressure and total enthalpy respectively. (x_n, y_n, z_n) is the unit vector normal to the surface from left to right side. AUSM scheme is based on the fact that the advection term and the pressure term can be upwinded separately. m and \tilde{p} are mass flux and pressure at the cell boundary which have different definition for different numerical scheme. Shima et al. has shown that AUSM and also other AUSM type schemes can be written in following form,

$$\tilde{\mathbf{F}} = \frac{m + |m|}{2} \Phi^L + \frac{m - |m|}{2} \Phi^R + \tilde{p}\mathbf{N} \quad (6)$$

where superscripts L and R show physical value at left and right side of cell boundary, and \tilde{p} is a mixing of pressure using Mach number of left and right state which is defined by,

$$\tilde{p} = \beta^+ p^L + \beta^- p^R \quad (7)$$

where

$$\beta^\pm = \begin{cases} \frac{1}{4}(2 \mp M^\pm)(M^\pm \pm 1)^2, & |M^\pm| < 1 \\ \frac{1}{2}(1 + \text{sign}(\pm M^\pm)), & \text{otherwise} \end{cases} \quad (8)$$

and

$$M^+ = \frac{V_n^L}{c}, \quad M^- = \frac{V_n^R}{c} \quad (9)$$

Roe's FDS is used for the mass flux in SHUS

schem:

$$m = \frac{1}{2} \left\{ (\rho V_n)^L + (\rho V_n)^R - |\bar{V}_n| \Delta \rho - \frac{|\bar{M} + 1| - |\bar{M} - 1|}{2} \bar{\rho} \Delta V_n - \frac{|\bar{M} + 1| + |\bar{M} - 1| - 2|\bar{M}|}{2\bar{c}} \Delta p \right\} \quad (10)$$

here $\Delta q = q^R - q^L$, and \bar{c} etc are the averages of the left and right side values.

By choosing the interpolation method for the values of primitive variables at each side of the cell boundary, a scheme with any spatially desired accuracy can be constructed. A compact 4th-order spatial accurate scheme is realized by using following MUSCL-TVD interpolations as proposed by Yamamoto et al. (Ref. 10):

$$q_{i+1/2}^L = q_i + \frac{1}{6} (\Delta^* \bar{q}_{i-1/2} + 2\Delta^* \tilde{q}_{i+1/2}), \quad (11)$$

$$q_{i+1/2}^R = q_{i+1} - \frac{1}{6} (2\Delta^* \bar{q}_{i+1/2} + \Delta^* \tilde{q}_{i+3/2}) \quad (12)$$

where

$$\begin{aligned} \Delta^* \bar{q}_{i-1/2} &= \min \text{mod} [\Delta^* q_{i-1/2}, b\Delta^* q_{i+1/2}], \\ \Delta^* \tilde{q}_{i+1/2} &= \min \text{mod} [\Delta^* q_{i+1/2}, b\Delta^* q_{i-1/2}], \\ \Delta^* \bar{q}_{i+1/2} &= \min \text{mod} [\Delta^* q_{i+1/2}, b\Delta^* q_{i+3/2}], \\ \Delta^* \tilde{q}_{i+3/2} &= \min \text{mod} [\Delta^* q_{i+3/2}, b\Delta^* q_{i+1/2}] \end{aligned}$$

and

$$\begin{aligned} \Delta^* q_{i+1/2} &= \Delta q_{i+1/2} - \frac{1}{6} \Delta^3 \bar{q}_{i+1/2}, \\ \Delta^3 \bar{q}_{i+1/2} &= \Delta \bar{q}_{i-1/2} - 2\Delta \bar{q}_{i+1/2} + \Delta \bar{q}_{i+3/2}, \end{aligned}$$

with

$$\begin{aligned} \Delta \bar{q}_{i-1/2} &= \min \text{mod} [\Delta q_{i-1/2}, b_1 \Delta q_{i+1/2}, b_1 \Delta q_{i+3/2}], \\ \Delta \bar{q}_{i+1/2} &= \min \text{mod} [\Delta q_{i+1/2}, b_1 \Delta q_{i+3/2}, b_1 \Delta q_{i-1/2}], \\ \Delta \bar{q}_{i+3/2} &= \min \text{mod} [\Delta q_{i+3/2}, b_1 \Delta q_{i-1/2}, b_1 \Delta q_{i+1/2}], \end{aligned}$$

and

$$\Delta q_{i+1/2} = q_{i+1} - q_i.$$

The operator “minmod” made up of two parts. When the arguments of the operator are of different signs, the value returned by the operator is zero. When the arguments are of same sign, the operator returns with the value of smallest absolute value. For two arguments,

$$\min \text{mod}[x, y] = S \cdot \max[0, \min\{|x|, S \cdot y\}]$$

and for three arguments,

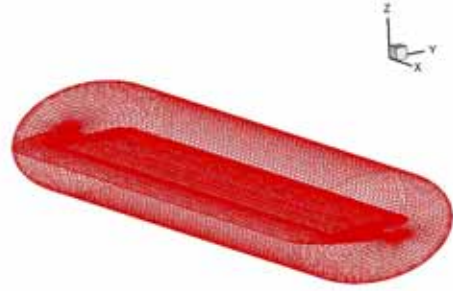
$$\min \text{mod}[x, y, z] = S \cdot \max[0, \min\{|x|, S \cdot y, S \cdot z\}]$$

here

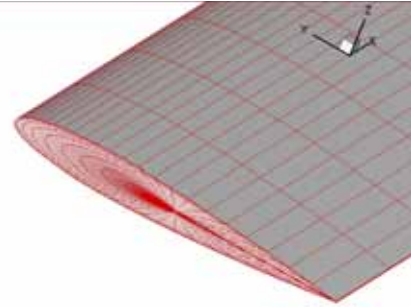
$$S = \text{sign}(x)$$

b and b_1 are the so-called “compression” parameter in the limiter. In current calculations, $b=4$ and $b_1=2$ were specified.

The so-called SOH type blade grid is used in this study. There is a singular line on the blade tip end and the grid is of O-type in the chordwise direction. A sample of the SOH-type grid around a rectangular tip end blade is shown in figure 1.



(a) Overall grid surrounding blade



(b) Grid points on the blade tip

Figure 1: SOH type blade grid

With SOH type blade grid, the blade shape fidelity is kept and the $k=1$ surface is consistent with the blade surface to allow easier boundary condition application.

As shown in Figure 2, a moving overlapped grid system is used for this study. Ground boundary condition is applied to the bottom surface of the outer background grid. The height of the rotor from the ground is simulated by changing the position of the bottom surface relative to the center of the rotor. HART II rotor model (Ref. 11) which simulates the main rotor of BO-105 helicopter is used conveniently for this study. Rotor height h_R is changed from $0.6R$ to $3R$ and also an out-of-ground effect case is calculated for reference as shown in Table 1.

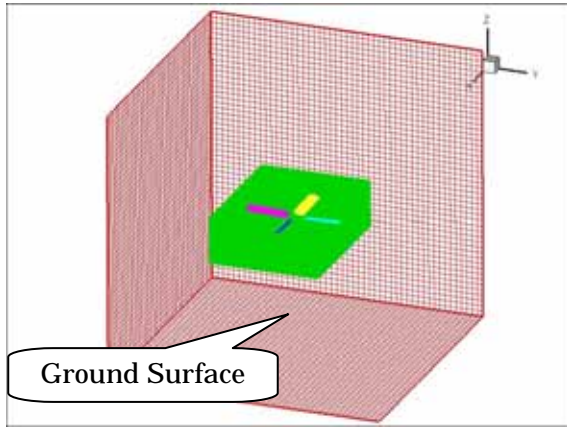


Figure 2: Overlapped grid system used for ground effect simulation

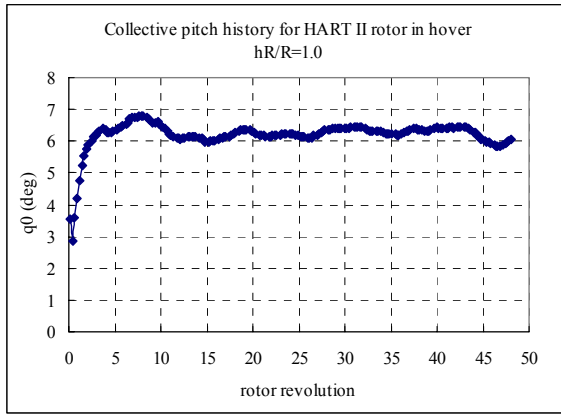


Figure 3: Collective pitch angle adjustment history, $h_R/R=1.0$

Table 1: IGE computation cases

Case No.	h_R/R	CFD Domain
1	0.6	-6.0 X/R 6.0 -6.0 Y/R 6.0 $-h_R/R$ Z/R 3.0
2	0.8	
3	0.9	
4	1.0	
5	1.2	
6	1.5	
7	2.0	
8	3.0	
9	OGE	

During the computation, the collective pitch angle of the rotor is adjusted every 90 degrees to keep the averaged thrust per revolution equal to the target thrust. A sample of the time histories of collective pitch angle adjustment for rotor height h_R/R of 1.0 is shown in Figure 3. The

rotor blades abruptly start to rotate at a constant speed at the beginning of the computation. As can be seen from Figure 3, the ground effect is felt by the blade at about 7 rotor revolutions where smaller pitch angle is enough to produce a same thrust in this case. The collective pitch angles and required torque corresponding to different rotor height is obtained under a constant thrust condition as shown in Table 2.

Table 2: Computation conditions of HART II rotor model in hover

HART Model	
Rotor Radius	$R=2m$
Blade chord	$c=0.121m$
Blade number	$N_{BLD}=4$
Freestream Mach number	$M = 0.0$
Hovering tip Mach number	$M_{tip}=0.6347$
Rotation speed	$\Omega=109.12rad/s$
Advance ratio	$\mu = 0.0$
Rotor height from ground	$h_R/R=0.6 \sim 3.0$
Thrust	$T=3300N$
	$C_T=0.004574$
	$C_T/\sigma=0.004574$

The history of thrust changes for $h_R/R=1.0$ is shown in Figure 4. Where thrust coefficient C_T is defined as

$$C_T = T / \rho A (R\Omega)^2 \quad (13)$$

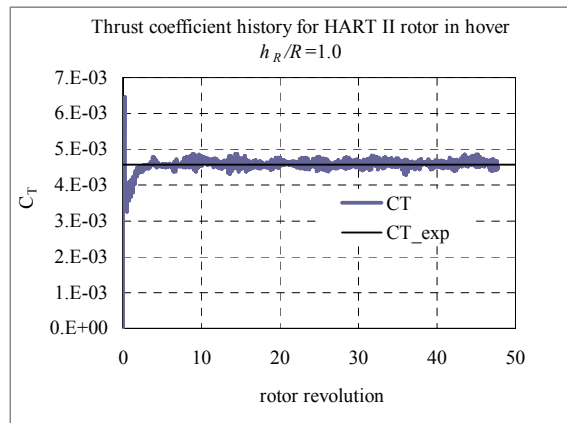


Figure 4: Thrust history for $h_R/R=1.0$

It can be seen that the thrust is converged to the target thrust after 5 rotor revolutions.

History of the required torque is shown in Figure 5. Here the torque coefficient is defined as

$$C_Q = Q / \rho A (R\Omega)^2 R \quad (14)$$

Compared with the thrust history of Figure 4, torque and also collective pitch angle as shown in Figure 3 converge slower and fluctuation remains even after long period of computations (more than 50 rotor revolutions). Same phenomena also reported by Phillips and Brown (Ref. 12). The rotor flow structure grows and evolves at a long time-scale in ground effect and there may exist an low frequency unsteady nature of this flowfield where the time-scale depends on the rotor height. Further studies regarding the influences of boundary conditions, grid resolutions, and other numerical settings on this obtained flow unsteadiness is required. At this point, only nearly converged state is obtained for all the cases in ground effect. Error bars indicate the range between maximum and minimum of collective pitch angle and required power are added to the averaged values as shown in Figure 6 and Figure 7.

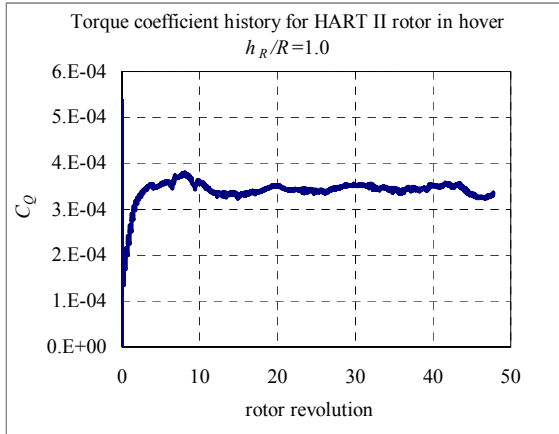


Figure 5: Torque history for $h_R/R = 1.0$

The final converged values of collective pitch angle with regard to various rotor heights are shown in Figure 6. Smaller collective pitch angle is required for lower rotor height which agrees with our existing empirical knowledge.

Figure 7 shows the calculated required power reduction from the OGE condition versus the rotor height. The result compares well with Cheeseman-Bennett's relation (Ref.13).

$$\left(\frac{P_{IGE}}{P_{OGE}} \right)_{T=const} = \frac{1}{1 + (R/4h_R)^2} \quad (15)$$

Hayden's empirical relation (Ref.14) defined as

$$\left(\frac{P_{IGE}}{P_{OGE}} \right)_{T=const} = \frac{1}{0.9926 + 0.03794(2R/h_R)^2} \quad (16)$$

is also shown in Figure 7. This empirical relation is based on the helicopter flight test data where the fuselage is exists. As can be seen from Figure 8, where the velocity vectors in the rotor center section are shown, there is a significant upwash area in the center part of the rotor which becomes stronger when the rotor height decrease, that should benefit the power consumption when a fuselage is located there.

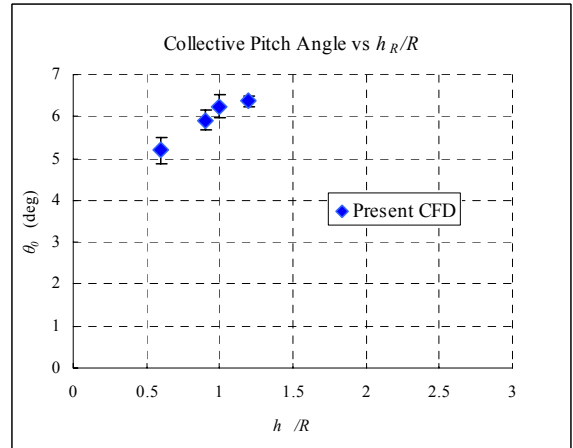


Figure 6: Required collective pitch angle vs rotor height, error bars indicate the range of max and min values

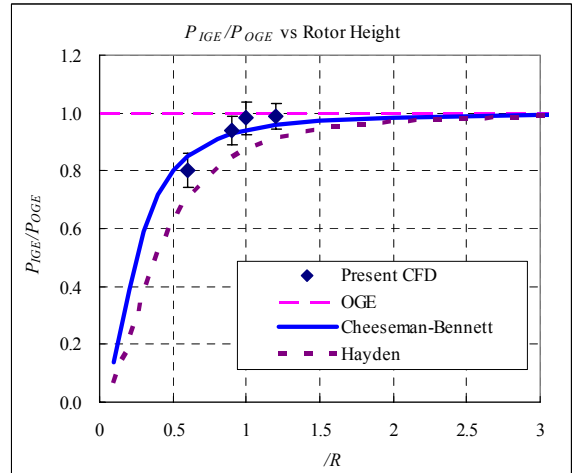


Figure 7: Required power change with rotor height, error bars indicate the range of max and min values

Velocity vectors at the rotor center section for $h_R/R = 1.0$ is shown in Figure 8. It can be seen the high speed flow is constrained in a thin layer along the ground surface which forms a wall jet.

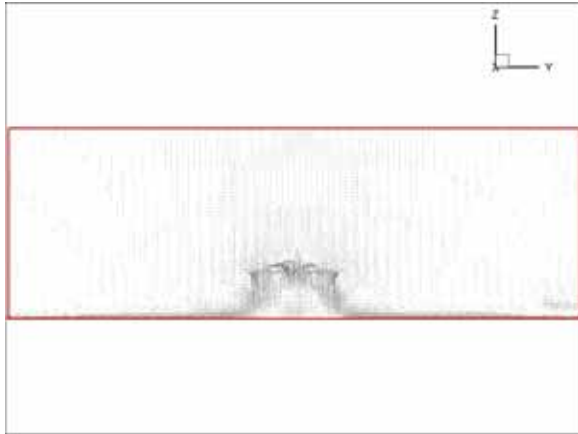


Figure 8: Velocity vectors in X plane for $h_R/R = 1.0$

An iso-vorticity plot for $h_R/R = 1.0$ at 20 rotor revolutions from start is shown in Figure 9. The starting vortex is expanding along the ground surface and gradually decreases in strength. Also a secondary strong vortex is formed on the ground which is generated by the collective pitch adjustment when the ground effect reach back to the rotor. A nearly converged solution for the rotor induced flowfield is obtained after this starting vortex goes out of the computation domain.

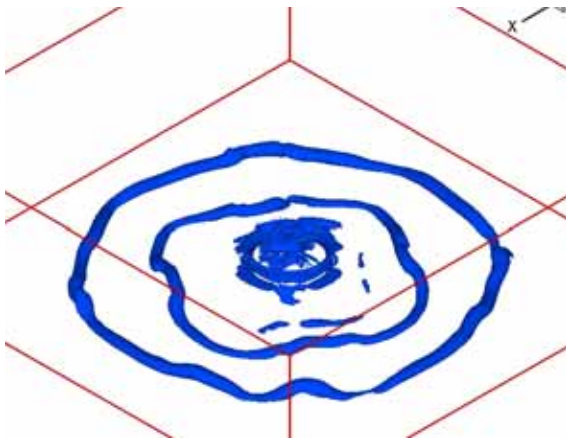


Figure 9: Iso-vorticity for $h_R/R = 1.0$ at 20 rotor revolutions

Velocity profiles calculated using the CFD Euler solver for $h_R/R = 1.0$ is shown in Figure 10. The velocity is nondimensionalized by the uniform induced velocity defined as

$$V_{i0} = \sqrt{\frac{T}{2\rho A}} = \sqrt{\frac{mg}{2\rho\pi R^2}} \quad (17)$$

Apparently, due to the neglect of the viscous effects in the CFD Euler solution, boundary layer

development on the ground surface for the wall jet can not be predicted. However, at the near positions from the rotor, the comparison of the CFD results with the experiment is quite well. But the comparison is poor for that at $X/R = 3.0$. This indicates that to correctly predict the flow away from the rotor, viscous effect becomes important, and Navier-Stokes solvers must be used for this problem. This will be a future works for this study. At this time, for the far-field flow where viscous effect must be taken into consideration, existing empirical results of a vertical jet blow are used.

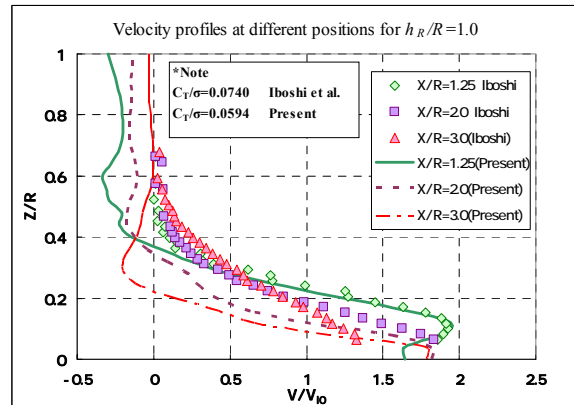


Figure 10: Comparison of velocity profiles between computation and experiment

The maximum radial velocity along the Y axis for $h_R/R = 1.0$ is plotted in Figure 11. It reaches a peak at near $2R$ away from the rotor center and then decreases gradually. Compared with existing experimental data, the decay rate is not low enough due to the lack of viscous dissipation. As will be discussed in next section, a modified vertical jet blow model agrees well with the experiments and this will be used for the proposed wall jet model for a hovering rotor.

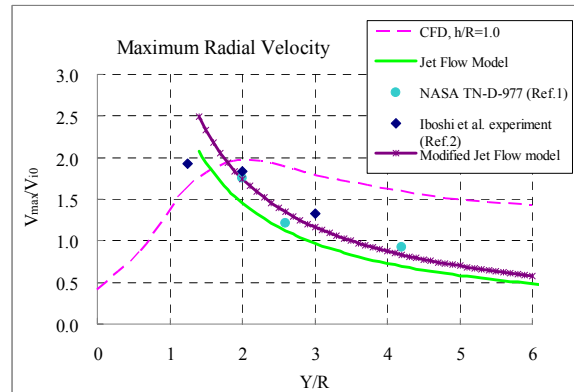


Figure 11: Maximum velocity in the wall jet

In the flow near the ground, caused by the rotating rotor, there is a tangential velocity component (whirl) as shown in Figure 12. This is a typical rotor induced flowfield feature differs from a simple vertical jet blow. This tangential velocity component is retained for the proposed wall jet model.

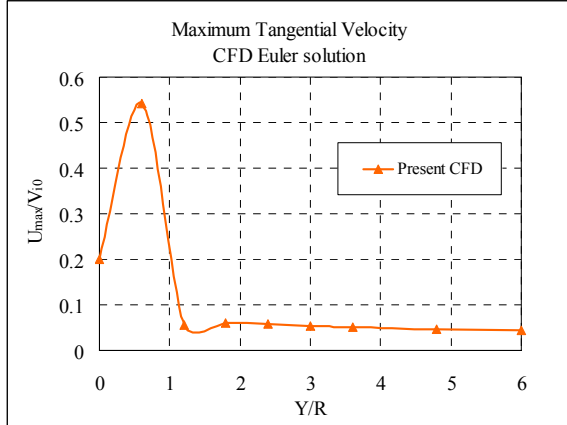


Figure 12: Maximum tangential velocity in the wall jet

Analogy to a vertical jet blowing model

As a simplest model for a rotor induced wall jet flow, we can consider it as a flow formed by an impinging vertical jet blow to a wall. For an axial jet blow impinging vertically to a wall, a wall jet along the wall is formed as illustrated in Figure 13.

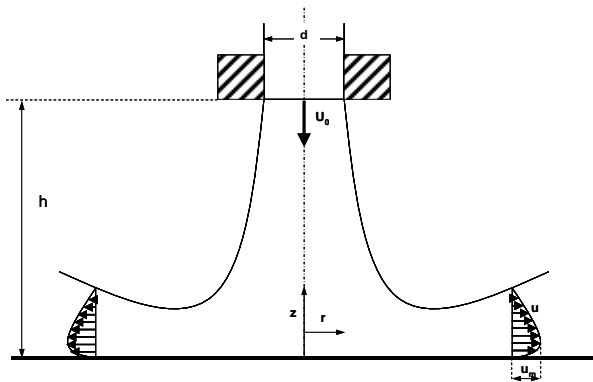


Figure 13: Axial jet blowing impingement model

The maximum speed u_m in the wall jet is given as a function of the distance from the jet center as

$$\frac{u_m}{U_0} = \frac{1.03}{\left(\frac{r}{d}\right)} \quad (18)$$

by Poreh et al. (Ref. 15) empirically. Here U_0 is the jet blowing speed. For a hovering helicopter rotor, we can take $U_0=2V_{i0}$. Also, d is the diameter of the jet blowing outlet. For a hovering rotor high enough from the ground and with ideal wake contraction, we can take $d=\sqrt{2}R$. But as can see in Figure 11, this gives an under-prediction of the u_m compared with experiments. It is modified to be $d=1.2\sqrt{2}R$ to meet with the experimental measurements. For a hovering rotor in ground effect, this factor may further need to be modified as a function of the rotor height. But at this point, there are not enough experimental and calculated data to establish such a relationship. So a simple wall jet model (WJM) caused by a hovering rotor is proposed regardless of the rotor height in this study.

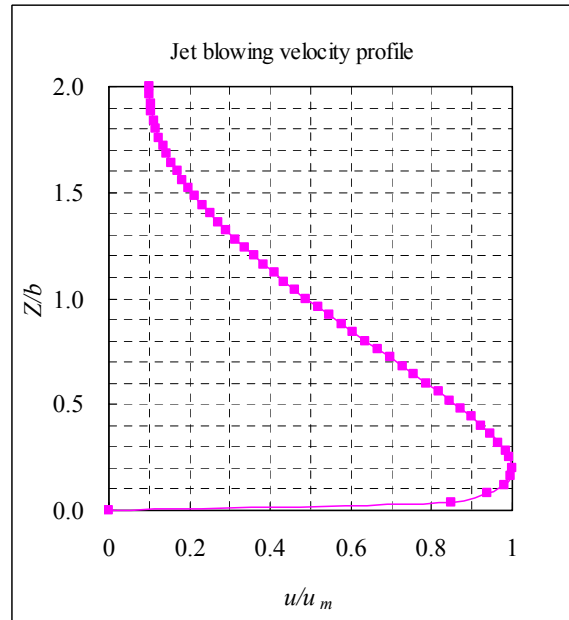


Figure 14: Velocity profile on the ground of wall jet induced by impinging axial symmetric jet blowing

A length scale b is also empirically defined as

$$b = 0.087r \quad (19)$$

which is referred as the vertical height where the speed is $u_m/2$.

The velocity profile for the wall jet caused by the axial vertical jet blow can be described as follows based on the experimental measurements:

$$\frac{u}{u_m} = \left(\frac{z}{b}\right)^{1/5} \left[0.39414 \left(2 - \frac{z}{b}\right)^2 + 0.0087055 \left(2 - \frac{z}{b}\right) + 0.087055 \right] \quad (20)$$

This formulae holds for $0 < z/b < 2$. The semi-similar velocity profile is shown in Figure 18.

Wall jet model for a hovering rotor

From above results and discussions, a simple wall jet model (WJM) caused by a hovering rotor is proposed. In the inner part around the rotor, results from CFD inviscid analysis are used. Away from the rotor, vertical jet blowing empirical relations are used while the whirl component from the CFD result is retained. This makes this model at the outer part differ from the simple vertical jet blowing flowfield. The positional relation of a moving ground vehicle with the rotor is defined in Figure 15.

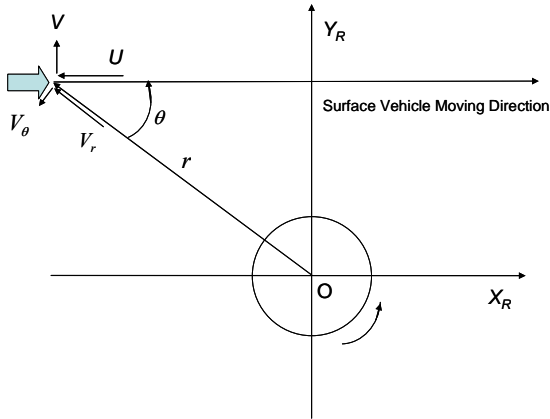


Figure 15: Position relation of a surface moving vehicle with rotor

To compute the wind in the vehicle-based axes, let U to be the maximum wind toward the head of the vehicle and V the maximum wind tangential to the vehicle from side, assume the wall jet maximum velocity components in the radial direction to be V_r and tangential direction to be V_θ , then

$$\begin{aligned} U &= V_r(r) \cos \theta + V_\theta(r) \sin \theta \\ V &= V_r(r) \sin \theta - V_\theta(r) \cos \theta \end{aligned} \quad (21)$$

When the vehicle position is at (X_R, Y_R) , then we have

$$\begin{aligned} r &= \sqrt{X_R^2 + Y_R^2} \\ \theta &= \pi - \tan^{-1} \left(\frac{Y_R}{X_R} \right) \end{aligned} \quad (22)$$

$V_r(r)$ is obtained by curve fitting in Figure 15 for the inner part as

$$\frac{V_r(r)}{V_{i0}} = a_6 \left(\frac{r}{R}\right)^6 + a_5 \left(\frac{r}{R}\right)^5 + a_4 \left(\frac{r}{R}\right)^4 + a_3 \left(\frac{r}{R}\right)^3 + a_2 \left(\frac{r}{R}\right)^2 + a_1 \left(\frac{r}{R}\right) + a_0 \quad (23)$$

where

$$\begin{aligned} a_6 &= -1.253 \times 10^{-5} \\ a_5 &= 6.815 \times 10^{-4} \\ a_4 &= -1.465 \times 10^{-2} \\ a_3 &= 0.1568 \\ a_2 &= -0.8607 \\ a_1 &= 2.129 \\ a_0 &= 5.022 \times 10^{-3} \end{aligned}$$

For $r/R > 1.8$, relations from vertical jet blowing is used with application to a hovering rotor with modified blowing outlet diameter as

$$\frac{V_r(r)}{V_{i0}} = \frac{3.496}{r/R} \quad (24)$$

And for V_θ component, we have

$$\frac{V_\theta(r)}{V_{i0}} = b_6 \left(\frac{r}{R}\right)^6 + b_5 \left(\frac{r}{R}\right)^5 + b_4 \left(\frac{r}{R}\right)^4 + b_3 \left(\frac{r}{R}\right)^3 + b_2 \left(\frac{r}{R}\right)^2 + b_1 \left(\frac{r}{R}\right) + b_0 \quad (25)$$

$$\text{for } 0 \leq \left(\frac{r}{R}\right) \leq 2$$

$$\begin{aligned} b_6 &= 0.7812 \\ b_5 &= -5.2705 \\ b_4 &= 12.999 \\ b_3 &= -13.574 \\ b_2 &= 4.5165 \\ b_1 &= 0.5241 \\ b_0 &= 0.2167 \end{aligned}$$

$$\text{and for } 2 < \left(\frac{r}{R}\right)$$

$$\begin{aligned} b_6 &= -1.873 \times 10^{-7} \\ b_5 &= 9.318 \times 10^{-6} \\ b_4 &= -1.799 \times 10^{-4} \\ b_3 &= 1.673 \times 10^{-3} \\ b_2 &= -7.363 \times 10^{-3} \\ b_1 &= 9.244 \times 10^{-3} \\ b_0 &= 6.080 \times 10^{-2} \end{aligned}$$

The velocity profile on the wall is assumed to be that from equation(20).

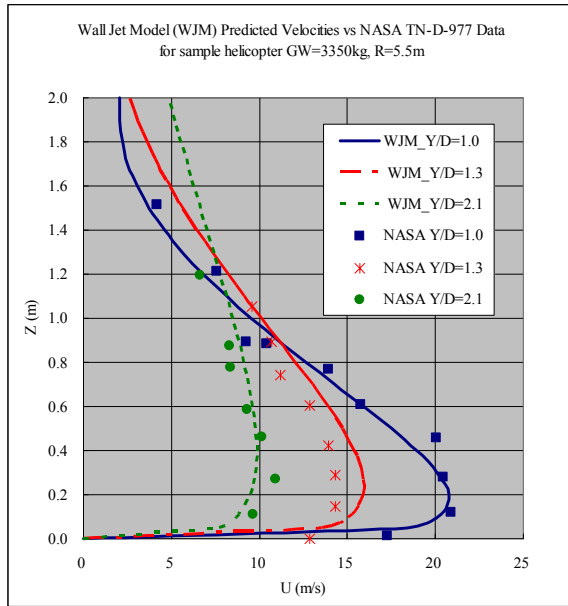


Figure 16: Comparison of proposed wall jet model with experiment

Velocity profiles predicted by above wall jet model are compared with dimensionalized measurement results in Ref.1 in Figure 16. A helicopter with gross weight of 3350 kg and rotor radius of 5.5 m is taken as a typical sample of EMS helicopters. The agreement between the proposed wall jet model and experimental measurement is reasonably well.

Simulated winds encountered by a ground vehicle moving at a straight line with distance of 11m (2R) are shown in Figure 17 when above sample helicopter is in hovering flight. At height of 0.5m, maximum side wind of 17m/s is expected. When the distance is 22m (4R) away from the rotor center, this wind decreases to 10 m/s and the difference between the height get smaller.

The wall jet model proposed here is simple to be incorporated into a driving simulator where further studies concerning the ground traffic safety influenced by downwash from a hovering helicopter can be carried out.

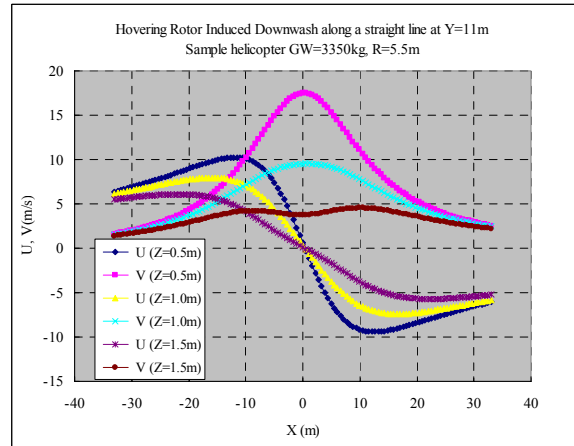


Figure 17: Wind speed change at different height along a line 11m away from a hovering helicopter (GW=3350kg, R=5.5m) as predicted by proposed wall jet model

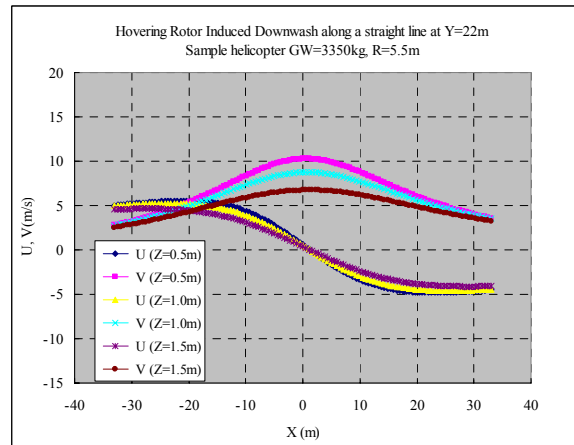


Figure 18: Wind speed change at different height along a line 22m away from a hovering helicopter (GW=3350kg, R=5.5m) as predicted by proposed wall jet model

Concluding remarks

Downwash caused by hovering rotor in ground effect is studied with emphasis on its influence on ground traffic.

With a Euler solver, rotor in ground effect is simulated and the obtained power merit curve for an isolated rotor agreed with the Cheeseman-Bennett relation.

The flow along the ground obtained by the Euler solver differs from experiment away from the rotor where boundary layer develops along the ground becomes dominant and for further CFD studies, viscous effect must be taken into

consideration for this part of flow.

A Wall Jet Model (WJM) is proposed for the flowfield induced by a hovering rotor which is simple and easy to be incorporated into a driving simulator for ground vehicles to study the safety problem influenced by the downwash of a helicopter. This model is composed with inviscid CFD results at near-field and a modified relation based on experimental results of vertical jet blow for the far-field on the ground.

Fuselage can have strong influence on the near-field flow structure and was not taken into account for current study. Further CFD studies include the viscous effect and fuselage could give more accurate and detailed flowfield

Acknowledgments

The authors would like to acknowledge all the members who participated the ATEC working group for "Research on the Influence of Helicopter Downwash to Ground Traffics". Members are from the major helicopter operators and research institutes in Japan. Professor Iboshi of Japan National Defense Academy provided his experimental data for comparisons. Without their inspiration and advice, this study would not be initiated.

References

1. O'Bryan, T., An Investigation of the effect of downwash from a VTOL aircraft and a helicopter in the ground environment, NASA TN D-977, 1961.
2. Iboshi N., Usuda H. and Itoga N., Ground effect of a hovering rotor over confined area, 45th Aircraft Symposium, Kitakyushu, Japan, October 10-12, 2007. (In Japanese).
3. Lee, T.E., Leishman, J.G. and Ramasamy, M., Fluid dynamics of interacting blade tip vortices with a ground plane, 64th Annual Forum of AHS, Montreal, Canada, April 29-May 1, 2008.
4. Tanabe, Y. and Saito, S., An integrated analysis code with CFD/rotor dynamics coupling developed in JAXA, AHS Specialists' Conference on Aeromechanics, San Francisco, CA, January 23-25, 2008.
5. Shima, E., and Jounouchi, T., Role of CFD in aeronautical engineering (No.14) - AUSM type upwind schemes - , NAL SP-34, 1999, pp.7-12.
6. Jameson, A., Schmidt, W., and Turkel, E., Numerical solutions of the Euler equations by finite volume method using Runge-Kutta time stepping schemes, AIAA Paper 81-1259, 1981.
7. Yee, H.C., and Harten, A., Implicit TVD schemes for hyperbolic conservation laws in curvilinear coordinates, AIAA Journal, Vol. 25, No.2, February 1987, pp.266-274.
8. Liou, M.S. and Steffen, C.J., A new flux splitting scheme, J. Comp. Phys. Vol.107, 1993, pp23-39.
9. Tanabe, Y., Saito, S., Yang, C., and Aoyama, T. Benoit, C., Gretay, J.-O., Jeanfaivre, G., Peron, S. and Sides, J., Inviscid numerical simulations of 2D parallel blade-vortex interaction – JAXA / ONERA cooperation, JAXA-RR-06-042E, March 2007.
10. Yamamoto, S. and Daiguji, H., Higher-order-accurate upwind schemes for solving the compressible Euler and Navier-Stokes equations, Computers & Fluids, Vol.22, No.2/3, pp.259-270, 1993.
11. Y.H. Yu, C. Tung, B. van der Wall, H.-J. Pausder, C. Burley, T. Brooks, P. Beaumier, Y. Delrieux, E. Mercker, and K. Pengel, The HART-II test: rotor wakes and aeroacoustics with Higher-Harmonic pitch Control (HHC) inputs - the joint German/French/Dutch/US project -, AHS 58th Annual Forum, Montreal, Canada, June 11-13, 2002.
12. Phillips C. and Brown R.E., Eulerian simulation of the fluid dynamics of helicopter brownout, AHS 64th Annual Forum, Montreal, Canada, April 29 - May 1, 2008.
13. Cheeseman I.C. and Bennett W.E., The effect of the ground on a helicopter rotor, R&M 3021, ARC, 1955.
14. Hayden J.S., The effect of the ground on helicopter hover power required, AHS 32nd Annual Forum, Washington, DC, May 1976.
15. Rajaratnam N., Turbulent Jets, Elsevier Scientific Publishing Company, Amsterdam, 1976.